Transverse Single-Spin Asymmetry for Diffractive Electromagnetic Jets with $p^{\uparrow} + p$ Collisions at $\sqrt{s} = 200$ GeV at STAR

The STAR Collaboration

Abstract

The STAR Collaboration reports the transverse single-spin asymmetry (A_N) for electromagnetic jets (EM-jets) at forward pseudorapidity ($2.8 < \eta < 3.8$) in diffractive events as a function of Feynman-x (x_F) and photon multiplicity in transversely polarized pp collisions at $\sqrt{s} = 200$ GeV. Results for A_N of single diffractive events, where the unpolarized proton stays intact, and semi-exclusive events, where the polarized proton stays intact, are presented. A_N for the single diffractive events is consistent with A_N for inclusive EM-jet production. Furthermore, the cross-section in single diffractive events compared to the inclusive events is small. The A_N in the semi-exclusive events has the opposite sign to the inclusive EM-jet A_N. These results show diffractive events can not make a significant contribution to the large A_N found for inclusive EM-jet production at forward pseudorapidity.

Keywords: Transverse single-spin asymmetry, single diffraction, cross-section

1. Introduction

Transverse single-spin asymmetry, also denoted as A_N, is the azimuthal asymmetry of the final state production of particles on the plane that spans the polarized proton spin direction and momentum direction. This asymmetry could be helpful in mapping out the three-dimensional proton structure [1]. Initially, it was predicted to be nearly zero in hard scattering processes in perturbative Quantum Chromodynamics (pQCD) [2]. However, various measurements on A_N for charged- and neutral-hadron production in proton-proton collisions showed sizeable asymmetries [1; 3; 4], contradicting the pQCD prediction. Since then, different models were proposed to unravel the origin of the large A_N observed in proton-proton collisions. Two major frameworks can provide potential explanations to such sizeable asymmetries. The first one is the transverse-momentum-dependent (TMD) framework, including the initial state Sivers effect and the final state Collins effect. The Sivers effect introduce the contribution of the large asymmetry from the correlation between the proton spin and the parton transverse momentum [5]. The Collins effect posits that the large A_N arises from the fragmentation process with the correlation between the spin of the fragmenting quark and the transverse momentum of the outgoing hadron [6]. The contribution from TMD framework is dominant when the momentum transfer ("hard" scale (Q)) is greater than the transverse momentum ("soft" scale (q_T)), $Q \gg q_T$ [7]. Another framework is based on the Twist-3 collinear factorization framework. The contribution of large A_N mainly comes from the spin-dependent twist-3 quark-gluon correlations, known as Efremov-Teryaev-Qiu-Sterman (ETQS) mechanism [8; 9]. Such twist-3 collinear factorization framework is contributed dominantly when $q_T \gg \Lambda_{QCD}$ and $Q \gg \Lambda_{QCD}$ [7]. However, in the region where $Q \gg q_T \gg \Lambda_{QCD}$, both frameworks give the same result [7].

In recent years, there were various experimental attempts on investigating the origin of A_N in the forward region in polarized proton-proton collisions [10; 11; 12; 13]. Among these studies, STAR [11] measured the forward π^0 A_N in two distinctive topology categories of the π^0 production. In one case, the π^0s are isolated, meaning a π^0 without any surrounding photons; while the other case looked at π^0s which are not isolated, meaning the π^0 is accompanied by other photons. The magnitude of the isolated π^0 A_N is significantly larger than that of the non-isolated case. Furthermore, the measurement at STAR on A_N for the electromagnetic jets (EM-jets) as a function of the EM-jet energy and photon multiplicity (number of photons inside the EM-jet) reveals that A_N has a strong dependency on the photon multiplicity [14]. Both behaviors suggested there might be additional sources of the contribution coming from other underlying processes. One of the proposed explanations is that the isolated π^0's are coming from the diffractive process [15].

Diffractive processes at RHIC are one of the essential tools to investigate the origin of the transverse single-spin asymmetries in polarized $p+p$ collisions, providing a unique approach to access the orbital motion of partons inside the proton [1]. One of the signatures of a diffractive process is a large rapidity gap and the vacuum quantum numbers transferred across the gap [16]. At the HERA experiment, about 15% of the total cross-section in $e + p$ is given by diffractive events [17]. In addition, the diffractive scattering events constitute about 25% of the total inelastic $p + p$ cross-section at the RHIC center-of-mass energies [18]. Studying the transverse single-spin asymmetries in diffractive processes would potentially allow us to study and understand the properties and the nature of the diffractive process in $p + p$ collisions [1].

This letter reports the results on the first measurement of transverse single-spin asymmetry for rapidity gap events and single diffractive events as a function of x_F ($x_F = \frac{2p_L}{\sqrt{s}}$). Furthermore, the fraction of the single diffractive process cross-section to the inclusive process cross-section at forward rapidity is studied. Finally, the transverse single-spin asymmetry for semi-exclusive events is studied. These studies could potentially provide evidence to develop and understand the diffractive physics in $p + p$ collisions.

2. The STAR Experiment

The STAR detector [19] is located at one of the collision points at Relativistic Heavy Ion Collider (RHIC) [20; 21]. RHIC is the world's leading collider, which can provide transversely or longitudinal polarized proton beams [22].

In this analysis, the Forward Meson Spectrometer (FMS) is used for detecting the photons at the forward region. The FMS is a lead-glass electromagnetic calorimeter located at about 7 meters away from the STAR interaction point (IP), covering a pseudorapidity region of about $2.6 < \eta < 4.1$. The FMS consists of two regions: an inner region ($3.3 < \eta < 4.1$) with smaller cells (size of each small cell 3.8 cm × 3.8 cm); and an outer region ($2.6 < \eta < 3.3$) with larger cells (size of each small cell 5.8 cm × 5.8 cm). Two types of triggers for the FMS are used in this analysis: the FMS Board Sum triggers, covering a 2x2 region of cells for both large and small cells, and the FMS Jet Patch triggers, which combine the board sum triggers to cover an area that is about a quarter of the entire detector size. Both triggers require the transverse energy sum for the corresponding regions exceed the threshold. Details of the FMS detectors and FMS triggers can be found in [11; 23].

The FMS reconstructs points or photon candidates by taking the energy from each cell and making contiguous groups of cells called clusters and then uses a moment analysis and shower shape fitting to finally reconstruct the point. Details for getting the points as photon candidates can be found in [11]. The calibration for FMS is using the π^0 reconstruction from points at FMS, since π^0 mostly decay to two photons.

The Roman Pot detectors (RP) are used to detect the slightly scattered protons in this analysis. The RP at STAR used for this analysis was upgraded with the RP used by the PP2PP experiment [24]. RPs are located on both sides of the STAR detector, where one side is at a position of about 15.8 meters and the other side is at 17.6 meters away from the STAR IP. Each set of RP consists of one RP station placed above the beam-line and another RP station placed below the beam-line. Every RP station contains four Silicon strip detector planes. With these two sets of RP, the proton momentum can be easily measured. Details of the RP setup can be found in [25; 26].

The Beam-Beam Counter (BBC) is a scintillator hodoscope which is used to trigger on minimum bias events, monitor the luminosity and measure the local polarimetry. The BBC is located on both sides of STAR, each at a position of about 3.75 meters away from the STAR IP. Each part of BBC consists of 6 small hexagonal scintillator tiles in the inner region, also called the small BBC region with $3.4 < |\eta| < 5.0$, and 12 large hexagonal scintillator tiles in the outer region, also called the large BBC region with $2.1 < |\eta| < 3.4$. Details of the BBC can be found in [27; 28].

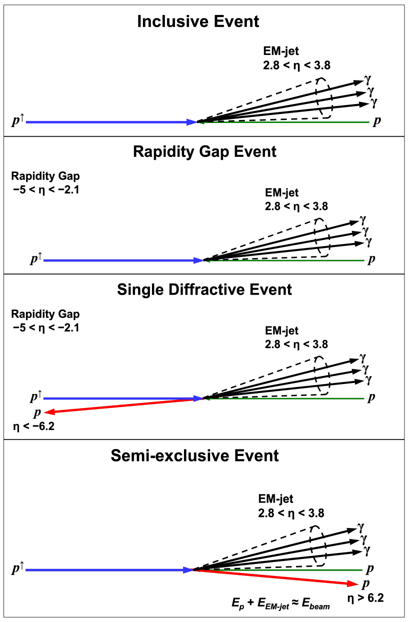

Figure 1: The schematic diagrams for four types of events mentioned in this Letter. From top to bottom, they are inclusive event, rapidity gap event, single diffractive event and semi-exclusive event.

In this analysis, the dataset with transversely polarized $p + p$ collisions at $\sqrt{s} = 200$ GeV collected at STAR in 2015 is used. The integrated luminosity of the dataset is about 52 pb^{-1}. The polarization for this dataset is measured using RHIC polarimeters [22]. The average polarization of the dataset is about 56.6 ± 1.7% [29].

3. Event selection

This analysis focuses on three different processes to extract A_N. These processes are: rapidity gap events, single diffractive events, and semi-exclusive events. Figure 1 shows the schematic diagrams for these classes of events including one not presented here but is used for comparison and that is inclusive events. The inclusive events are mentioned in (???). Rapidity gap events require one electromagnetic jet (EM-jet) at the FMS, and to ensure a rapidity gap, a veto on the east BBC (east BBC veto). The single diffractive events are a subset of the rapidity gap events so requiring the same FMS EM-jet reconstruction and east BBC veto; and then an additional requirement that there is one proton track in the east RP (unpolarized proton direction away from the FMS). The semi-exclusive process requires one EM-jet at the FMS, one proton track on west RP (polarized proton direction towards the FMS), a veto to satisfy the rapidity gap requirement using the west BBC, and a constraint on the sum of the energy for the EM-jet and proton to equal the beam energy (energy sum).

3.1. Electromagnetic jet reconstruction

An EM-jet is a jet reconstructed using FMS points. The EM-jet reconstruction criteria are the same among all the four types of events mentioned in this letter. In this analysis, only the

FMS points with $E > 1$ GeV are applied to the EM-jet reconstruction, in order to minimize the effect on the background noise. The EM-jet is reconstructed with the anti-k_T algorithm from the FastJet package [30], with the resolution parameter $R = 0.7$. In the jet reconstruction, the primary vertex position in the beam direction (z-direction) is determined according to the priority for the primary vertex obtained from the Time Projection Chamber (TPC) [31], Vertex Position Detector (VPD) [32], and BBC. The fraction of the primary vertex obtained from the TPC, VPD and BBC are about 1%, 33%, and 50%, respectively. The rest of the events that can not obtained from these three detectors are assigned the primary vertex in z-direction to be 0 cm. Only the events with primary vertex $|z| < 80$ cm are accepted. Two types of corrections are applied to the reconstructed EM-jets. The first type is the underlying event correction using the off-axis cone method, where it subtracts the background from soft scatterings [33]. The second type is the correction for the EM-jet energy from the detector level to the particle level. The correction function is studied based on the particle level and detector level simulation, detailed in 4.1. Furthermore, the EM-jet transverse momentum (p_T) is required to pass both the trigger threshold and the fixed threshold 2 GeV/c threshold. Lastly, only one EM-jet is accepted for rapidity gap event, single diffractive event, and semi-exclusive event.

3.2. Proton track selection

The proton in the single diffractive event is detected on the east side RP and is considered the unpolarized proton and negative pseudorapdity by STAR convention; it's direction is opposite to the FMS which is at positive pseudorapidity. The proton in the semi-exclusive event is detected on the west side RP and is considered the polarized proton and has the same pseudorapidy cardinality as the FMS. There is no requirement of a proton track in rapidity gap events. The selection criteria for the track in RP (RP track) is similar in both single diffractive events and semi-exclusive events. To begin with, the RP track is required to hit at least 7 silicon planes. Under this condition, the track hits two RP stations, and the position information for the hits can be reconstructed, which can be used to reconstruct the RP track. Details on the RP track reconstruction can be found in [26] Then, the RP track is further selected by its fiducial region on its θ_x, θ_y, p_x and p_y. θ_x and θ_y are the scattering angle in (x,z) plane and in the (y,z) plane, respectively. p_x and p_y are the x- and y-components of the RP track momentum, respectively. These fiducial region cuts are helpful in minimizing the beam backgrounds. Furthermore, the cuts on RP track ξ is applied. RP ξ is the fraction of proton momentum loss $\xi = \frac{p_{beam}-p_{RP}}{p_{beam}}$, where p_{beam} and p_{RP} is the momentum of the beam and the RP track respectively. The east RP track ξ in the single diffractive event is required to be within $0 < \xi < 0.15$, based on the requirements for the single diffractive process in experiment [16]. The west RP track ξ in the semi-exclusive event is required to within $0 < \xi < 0.45$. Lastly, one and only one RP track on east (west) side is allowed for single diffractive event (semi-exclusive event).

3.3. BBC veto

The BBC veto cuts mainly serve two purposes: minimizing accidental coincidences, and determining the rapidity gap. The accidental coincidences refer to multiple collision events, where the EM-jet is detected in one event while the proton track is detected in another. The BBC veto cuts focused on the east side BBC are used in the single diffractive events and rapidity gap events; the west side BBC veto cuts are for semi-exclusive events. The threshold for the sum of the small (large) tiles (ADC sum) depends on the minimum ionized particle hitting the corresponding BBC region. Only when both the ADC sum for the small tiles and the ADC sum for large tiles are less than these corresponding thresholds are events accepted. The east side BBC detector covers 3 pseudo-rapidity units, so the veto on the east side BBC is a sufficient to ensure a rapidity gap requirement for single diffractive events. However, the west BBC partially overlaps the same pseudorapidity as the FMS so semi-exclusive events can not be called diffractive events.

3.4. Energy sum cut

The energy sum cut id only applied to the semi-exclusive events, where the energy sum is the sum of the energy of the EM-jet and the west RP track. This cut is necessary because, as shown in Fig. 1, these types of events have both the proton and the jet going to the same side; therefore, the energy sum should be consistent with the beam energy within resolution. However, for the semi-exclusive events passing all other cuts mentioned above, two obvious peaks can be seen in the energy sum distributions, regardless of the region of the EM-jet energy. The lower energy sum peak centers around the beam energy, which should mostly consist of the real semi-exclusive events. The higher energy sum peak is far higher than the beam energy, which should mostly consist of the accidental events with the west RP track coming from the protons in either elastic scattering events or beam remanent. Therefore, the energy sum cut is based on the separation of two energy sum peaks and only the energy sum at the low peak region is accepted.

4. Simulation

4.1. Simulation on FMS

In this analysis, the simulation for the FMS is aiming to study the correction for the EM-jet energy from the detector level to the particle level. The particle level simulation uses PYTHIA6 with the tune setting of Perugia2012 (Tune parameter 370) [34; 35] to generate the proton-proton collisions with $\sqrt{s} = 200$ GeV. Then, the GEANT3 [36] based STAR detector simulation is applied to study the detector responses. Based on the results from the simulations, the two-dimensional profile for the energy of the EM-jet in the particle level to the energy of its best matched detector level EM-jet is made. A linear fit is applied for the detector level EM-jet at 7 - 60 GeV to study its general relation to the particle level. Such linear fit is used as the energy correction function to correct the EM-jet energy from detector level to particle level.

4.2. Single diffractive process simulation

The main goals for the single diffractive process simulation are to study the efficiency of the detectors with the single diffractive events as well as investigating the fraction of the single diffractive events in the rapidity gap events. The single diffractive events in simulation are generated using Pythia8 with the flag "SoftQCD:singleDiffractive" [37]. In this simulation, only the single diffractive events with single proton at $\eta < 0$ are considered. Then, the detector level simulations are processed for these single diffractive events. The first type of the detector level simulation is the GEANT3 [36] based STAR detector simulation. Another type is the GEANT4 [38] based Roman Pot detector simulation. Both detector level simulations are applied individually with the same single diffractive process simulation sample and synchronized event-by-event.

The east BBC efficiency and the east RP efficiency for the single diffractive event are studied based on the single diffractive process simulation. The east BBC efficiency is calculated by the fraction of the single diffractive process simulation events passing the east BBC veto that is same as data (rapidity gap events), showing in Sec. 3.3, to the generated single diffractive process events with proton $\eta < 0$. The relative uncertainty for the east BBC efficiency is calculated by deviations between PYTHIA8 and HERWIG [39] models. The east BBC uncertainty is 99.8 ± 10.0%. The east RP efficiency is calculated by the fraction of the single diffractive process simulation events passing both east RP selection and east BBC veto (single diffractive events) to the generated single diffractive process events with proton $\eta < 0$. The relative uncertainty for east RP efficiency is up to 6.5%, according to [25]. Therefore, the east BBC efficiency is 11.4 ± 0.7%

The fraction of the single diffractive events in the rapidity gap events is also explored using calculations with data and simulation. In the data, the rapidity gap events consist of single diffractive events (RSD) and non-single diffractive events (NSD). It is not able to directly separate both types of events from the rapidity gap events. In the simulation, we calculate the fraction in Equ. 1,

$$frac(sim) = \frac{SD}{RSD} \tag{1}$$

which is the ratio of the number of the single diffractive events (SD) to the number of the rapidity gap events. Only single diffractive process events are generated in the simulation. In order to distinguish between rapidity gap events in data, these rapidity gap events in such simulation are called real single diffractive events (RSD). In data, the similar fraction is also calculated, showing in Equ. 2

$$frac(data) = \frac{SD}{RSD + NSD} \tag{2}$$

The purity of the single diffractive events (SD) in data is high, detailed in Sec. 5.1. We assume the fraction $\frac{SD}{RSD}$ in both data and simulation are the same. Combining both equations, we get the fraction of single diffractive events in rapidity gap events in data $\frac{RSD}{RSD+NSD}$ is 68.7 ± 0.6 ± 8.2%. It indicates that a large fraction of the rapidity gap events are single diffractive events. It provides another approach to investigate the transverse single-spin asymmetry for the single diffractive process using the $p^{\uparrow} + p$ collisions in 2022 and 2024 with STAR forward upgrade detectors.

5. Background

5.1. Accidental coincidence for the single diffractive events

The fraction of accidental coincidence of the single diffractive events is estimated using highly scaled data and selected only with the minimum bias triggers with STAR detectors. These events are called zero-bias events. Due to the low coincident rate of the FMS detector in the zero-bias events, most of the zero-bias events are without any FMS detector responses. Approximately 0.2% of the zero-bias events meet both criteria for east BBC veto and east RP track cuts. This is the rate for the accidental coincidence in the single diffractive process, and it is the same rate within every process.

In the single diffractive events, the fraction of the accidental coincidence ($frac_{AC}$) can be calculated using Equ. (3).

$$frac_{AC} = \frac{n_{AC}}{n_{SD}} = \frac{n_{AC}}{n_{RG}} \times \frac{n_{RG}}{n_{SD}} \tag{3}$$

In this equation, $\frac{n_{AC}}{n_{RG}}$ is the accidental coincidence rate, n_{RG} and n_{SD} is the number of rapidity gap events and measured single diffractive events per each EM-jet x_F bin, respectively. The fraction of the accidental coincidence in the single diffractive events is about 1.9%. Therefore, the fraction of real single diffractive events in the measured single diffractive events in data, is about 98.1%. Such effect on the accidental coincidence to the measured A_N is assigned to the systematic uncertainty.

5.2. Background for semi-exclusive events using mix event method

For the accidental coincidence in the semi-exclusive events, the energy sum is usually much higher than the beam energy because the west RP track is coming from the proton from non-diffractive events, especially from elastic scattering events. Therefore, in order to estimate the contribution to the semi-exclusive events from such background, the mixed event background method is used. In this method, the distribution for the west RP track energy in the zero-bias events and the distribution for the EM-jet energy from the inclusive process are applied to investigate the potential accidental coincidence background. Equation 4 shows the calculation of the mixed event energy sum (Esum(i+j)) per energy bin.

$$Esum(i + j) = \sum_{i,j} P(i) \times n(j) \tag{4}$$

P(i) is the fraction of EM-jet yields in the inclusive EM-jet energy distribution for [i,i+1] (GeV) within each specific x_F range. n(j) is the yield of west RP energy distribution for [j,j+1] (GeV) for the zero-bias events. All the possible combinations are considered and accumulated in the mixed event energy sum background calculation. The shape of the mixed event energy background per EM-jet x_F region is then scaled to the maximum value of the accidental coincidence region (the higher peak region in the energy sum spectrum). The fraction of accidental coincidence to semi-exclusive events in data can be calculated as the ratio of the integrated yields for the scaled mixed event energy sum background within the signal region to the integrated yields for semi-exclusive events in the data within the signal region, where the signal region is the energy sum cut region defined in Sec. 3.4. The accidental coincidence fraction is small (less than 3%), so its effects on the A_N are assigned to systematic uncertainty for the semi-exclusive events.

6. Systematic uncertainty

The systematic uncertainty for the transverse single-spin asymmetry consists of two types of contribution: the effects due to the threshold determined in the event selection and the effects due to the accidental coincidence background. The former type is considered for all these three types of events. The major idea is varying the thresholds for the BBC veto for these three types of events and the energy sum cut for the semi-exclusive events. Each of the threshold change about 10 - 20% to test its effects on the A_N as well as its statistical uncertainty. The systematic uncertainty for each type of threshold are calculated independently. In addition, the events passing one trigger related to FMS where they might contain some fraction of the beam remnant background are excluded. For these term related to the event selection criteria or the triggers, the Barlow check in Bayesian method is applied to all of these terms to consider whether to take into account for the final systematic uncertainty [40]. Another type of the systematic uncertainty is related to the accidental coincidence, where they are discussed in Sec. 5.1 for the single diffractive events and in Sec. 5.2 for the semi-exclusive events. In this analysis, the systematic uncertainty for the transverse single-spin asymmetry are calculated independently for each x_F bin.

7. Results

7.1. Cross-ratio method

The cross-ratio method is applied to extract the A_N in this analysis [41]. The final state productions in the transversely polarized proton-proton collisions with the polarized proton spin "up" ("down") can be expressed in Equ. 5 and 6.

$$N^{\uparrow}(\phi) = \epsilon\mathcal{L}\,(1 + P \times A_N \cos(\phi))\,\sigma_0 \tag{5}$$

$$N^{\downarrow}(\phi) = \epsilon\mathcal{L}\,(1 - P \times A_N \cos(\phi))\,\sigma_0 \tag{6}$$

In both equation, the final state productions ($N^{\uparrow}$, $N^{\downarrow}$) can be expressed as a function of the azimuthal angle ϕ. ϵ stands for the detector efficiency, $\mathcal{L}$ is the luminosity, P is the polarization of the transversely proton beam. Equation 7 shows the cross-ratio method calculation, which combines both Equ. 5 and 6.

$$P \times A_N \cos(\phi) = \frac{\sqrt{N^{\uparrow}(\phi)N^{\downarrow}(\phi+\pi)} - \sqrt{N^{\downarrow}(\phi)N^{\uparrow}(\phi+\pi)}}{\sqrt{N^{\uparrow}(\phi)N^{\downarrow}(\phi+\pi)} + \sqrt{N^{\downarrow}(\phi)N^{\uparrow}(\phi+\pi)}} \tag{7}$$

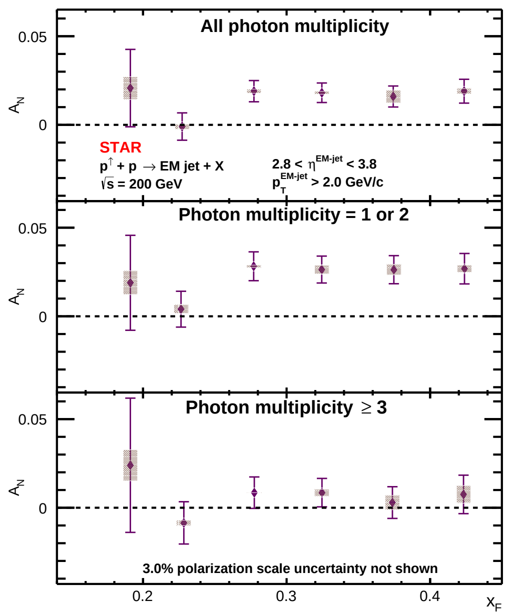

Figure 2: A_N for the rapidity gap events as a function of EM-jet x_F with three cases of photon multiplicity: all photon multiplicity (top), one- or two-photon multiplicity (mid) and three- or more-photon multiplicity (bottom). The statistical uncertainty is shown in bar, while the systematic uncertainties shown in shaded box.

This method cancels out the effects on the non-uniform detector efficiency and the time-dependent luminosity at leading order. In this study, 16 ϕ bins are applied in full 2π azimuthal region, resulting in 8 data points in calculation. Based on this method, the cosine fit is used for these 8 points to extract the A_N.

7.2. Transverse single-spin asymmetry for rapidity gap events

Figure 2 shows the A_N for the rapidity gap events as a function of EM-jet x_F with three cases of photon multiplicity: all photon multiplicity, one- or two-photon multiplicity and three- or more-photon multiplicity. The photon multiplicity refers to the number of photons inside the EM-jets. A two tails student-test (t-test) is applied to investigate the non-zero significance for the A_N for the rapidity gap events for EM-jet with one- or two-photon multiplicity and three- or more-photon multiplicity. The former one shows its overall non-zero with more than 99.9% confidence level, while the later one only shows with more than 90% confidence level. Furthermore, the A_N for the rapidity gap events for EM-jet with one- or two-photon multiplicity is much larger than that with 3- or more- photon multiplicity at $0.25 < x_F < 0.45$.

7.3. Transverse single-spin asymmetry for single diffractive events

Figure 3 shows the A_N for the single diffractive events as a function of EM-jet x_F with three cases of photon multiplicity which are same as rapidity gap events. The non-zero significance for the A_N for the single diffractive with one- or two-photon multiplicity EM-jets is at 99% confidence level. Furthermore, the A_N for the single diffractive events for EM-jet

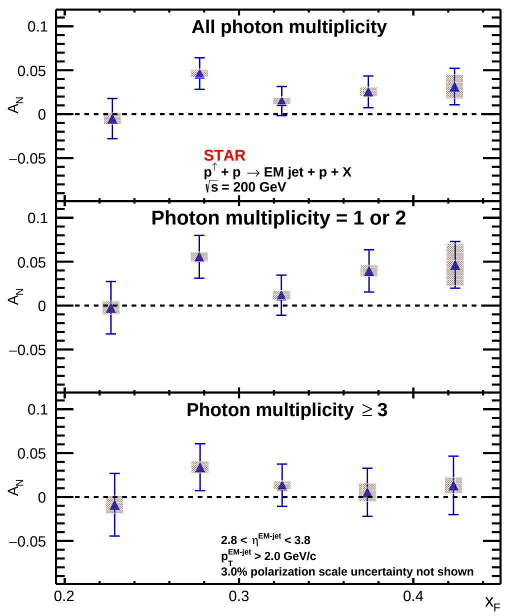

Figure 3: A_N for the single diffractive events as a function of EM-jet x_F with three cases of photon multiplicity: all photon multiplicity (top), one- or two-photon multiplicity (mid) and three- or more-photon multiplicity (bottom). The statistical uncertainty is shown in bar, while the systematic uncertainties shown in shaded box.

with one- or two-photon multiplicity is much larger than that with three- or more- photon multiplicity at $0.25 < x_F < 0.45$.

7.4. Contribution for the single diffractive events to inclusive events

In order to understand the contributions for A_N from the single diffractive events to A_N from the inclusive events, the fraction of the cross-section in the single diffractive events to the inclusive events is first studied. Since it is difficult to calculate the efficiency of the FMS detector and the triggers, only the cross-section fraction is calculated. Both the analyses of A_N for inclusive events (cite???) and the single diffractive events apply the same dataset, same list of triggers. Therefore, the efficiency of the FMS detector and the triggers can be canceled out when calculating the cross-section fraction. Equation 8 shows the calculation of cross-section fraction.

$$\frac{\sigma_{SD}}{\sigma_{inc}} = \frac{N_{SD} \times purity}{N_{inc} \times \varepsilon_{RP} \times \varepsilon_{BBC}} \tag{8}$$

Purity can be calculated using the zero-bias events, detailed in Sec. 5.1. The efficiency of RP (ε_{RP}) and east BBC (ε_{BBC}) can be calculated from simulation, detailed in Sec. 4.2. N_{SD} and N_{inc} are the number of single diffractive events and inclusive events, respectively. The overall cross-section fraction for the entire dataset is 0.586% ± 0.070%.

The differential cross-section fraction is studied as a function of EM-jet x_F, shown in Fig. 4. The single diffractive process cross-section is very small compared to the inclusive process cross-section, which shows that it can not provide significant contribution to the large A_N in inclusive process.

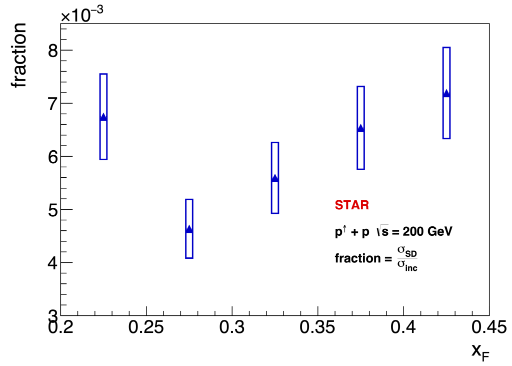

Figure 4: Cross section fraction of the single diffractive process (σ_{SD}) to the inclusive process (σ_{inc}) as a function of x_F.

Furthermore, to better visualize the A_N contributions of the single diffractive events and the rapidity gap events to the inclusive events, a direct comparison plot among the A_N for inclusive events, rapidity gap events, and single diffractive events for one or two-photon multiplicity, and three or more-photon multiplicity are shown in Fig. 5. Applying the two tailed t-test between the A_N for every two types of events, the A_N for the single diffractive events and the rapidity gap events are consistent with that for inclusive events within uncertainty for both multiplicity cases. These direct comparison results indicate that the single diffractive events can not provide evidence that it contributes to the large A_N in the inclusive events.

7.5. Transverse single-spin asymmetry for semi-exclusive events

Figure 6 shows the A_N for the semi-exclusive events as a function of EM-jet x_F with the one- or two-photon multiplicity EM-jets. For the EM-jet in the semi-exclusive events, most of them are with one- or two-photon multiplicity. Therefore, only this type of the EM-jet photon multiplicity is considered in the study. Constant fit is applied to check the n-sigma significance for non-zero A_N value among these x_F regions. It shows that the A_N of the semi-exclusive process is more than 3σ significance to be non-zero. However, the semi-exclusive EM-jet A_N is negative, which is different from A_N either in inclusive events or in single diffractive events. Further theories are needed to understand this sign change.

8. Summary and conclusions

We present the first measurements of the transverse single-spin asymmetry for the single diffractive events and rapidity gap events for transversely polarized $p + p$ collisions at $\sqrt{s} = 200$ GeV at the STAR experiment. About two-thirds of the rapidity gap events are single diffractive events, and both measurements reveal a dependency on A_N to the EM-jet photon multiplicity, consistent with previous studies on the inclusive π^0 and EM-jet A_N at STAR. Furthermore, The A_N values for the single diffractive events where the unpolarized proton remains intact are consistent with A_N for inclusive events within uncertainty, showing that the single diffractive events can not explain the large A_N in inclusive EM-jet events. The fraction of the single diffractive cross-section to the inclusive cross-section at forward pseudorapidity is 0.586% ± 0.070% provides evidence for potential theories regarding A_N for diffractive events. Due to the tiny cross-section fraction, the single diffractive events can not have a major contribution to the large A_N in inclusive EM-jet events. The A_N value for semi-exclusive events where the polarized proton remains intact is negative; therefore it too can not contribute to the large positive A_N in the inclusive EM-jet events. However, further theories are needed to understand this negative value for the semi-exclusive events.

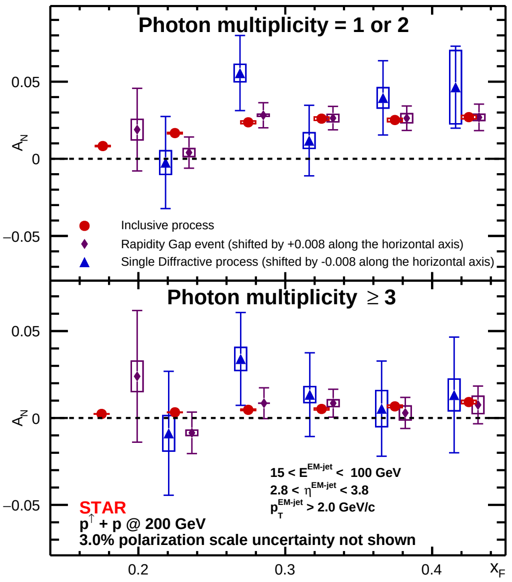

Figure 5: A_N for inclusive events (red), the rapidity gap events (purple) and single diffractive events (blue) as a function of x_F for one- or two-photon multiplicity case (top panel) and three- or more-photon multiplicity (bottom panel). The A_N for single diffractive events shifts -0.008 along the x-axis, and the A_N for rapidity gap events shifts +0.008 along the x-axis

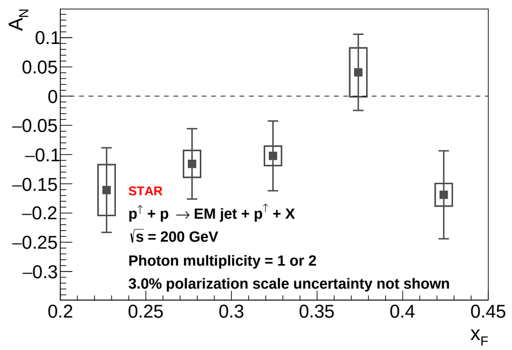

Figure 6: A_N for the one- or two-photon multiplicity EM-jet in the semi-exclusive events as a function of x_F. The statistical uncertainty is shown in bar, while the systematic uncertainties shown in shaded box.

Acknowledgements

To be included later.....

References

[1] Elke-Caroline Aschenauer et al. The RHIC Cold QCD Plan for 2017 to 2023: A Portal to the EIC. 2 2016.

[2] G. L. Kane, J. Pumplin, and W. Repko. Transverse quark polarization in large-p_T reactions, e^+e^- jets, and leptoproduction: A test of quantum chromodynamics. *Phys. Rev. Lett.*, 41:1689–1692, Dec 1978.

[3] R. D. Klem, , et al. Measurement of asymmetries of inclusive pion production in proton-proton interactions at 6 and 11.8 gev/c. *Phys. Rev. Lett.*, 36:929–931, Apr 1976.

[4] D.L. Adams et al. Comparison of spin asymmetries and cross sections in 0 production by 200 gev polarized antiprotons and protons. *Physics Letters B*, 261(1):201–206, 1991.

[5] Dennis Sivers. Single-spin production asymmetries from the hard scattering of pointlike constituents. *Phys. Rev. D*, 41:83–90, Jan 1990.

[6] John Collins. Fragmentation of transversely polarized quarks probed in transverse momentum distributions. *Nuclear Physics B*, 396(1):161–182, 1993.

[7] Xiangdong Ji, Jian-Wei Qiu, Werner Vogelsang, and Feng Yuan. Unified picture for single transverse-spin asymmetries in hard-scattering processes. *Phys. Rev. Lett.*, 97:082002, Aug 2006.

[8] A.V. Efremov and O.V. Teryaev. Qcd asymmetry and polarized hadron structure function measurement. *Physics Letters B*, 150(5):383–386, 1985.

[9] Jianwei Qiu and George Sterman. Single transverse spin asymmetries. *Phys. Rev. Lett.*, 67:2264–2267, Oct 1991.

[10] J. Adam and all. Comparison of transverse single-spin asymmetries for forward π^0 production in polarized pp, pAl and pAu collisions at nucleon pair c.m. energy $\sqrt{s_{NN}}$ = 200GeV. *Phys. Rev. D*, 103:072005, Apr 2021.

[11] J. Adam and all. Measurement of transverse single-spin asymmetries of π^0 and electromagnetic jets at forward rapidity in 200 and 500 gev transversely polarized proton-proton collisions. *Phys. Rev. D*, 103:092009, May 2021.

[12] M. H. Kim and all. Transverse single-spin asymmetry for very forward neutral pion production in polarized $p + p$ collisions at $\sqrt{s}$ = 510GeV. *Phys. Rev. Lett.*, 124:252501, Jun 2020.

[13] N. J. Abdulameer and all. Transverse single-spin asymmetry of charged hadrons at forward and backward rapidity in polarized $p + p$, p + Al, and p + Au collisions at $\sqrt{s_{NN}}$ = 200GeV. *Phys. Rev. D*, 108:072016, Oct 2023.

[14] Mriganka Mouli MONDAL. Measurement of the Transverse Single-Spin Asymmetries for π^0 and Jet-like Events at Forward Rapidities at STAR in $p + p$ Collisions at $\sqrt{s}$ = 500 GeV. *PoS*, DIS2014:216, 2014.

[15] Elke-Caroline Aschenauer and all. The rhic spin program: Achievements and future opportunities, 2015.

[16] R. L. Workman et al. Review of Particle Physics. *PTEP*, 2022:083C01, 2022.

[17] The H1 and ZEUS Collaborations. Combined inclusive diffractive cross sections measured with forward proton spectrometers in deep inelastic ep scattering at hera. *The European Physical Journal C*, 72(10):2175, 2012.

[18] V. Khachatryan and all. Measurement of diffractive dissociation cross sections in pp collisions at $\sqrt{s}$ = 7TeV. *Phys. Rev. D*, 92:012003, Jul 2015.

[19] K.H. Ackermann *et al.* Star detector overview. *Nuclear Instruments and Methods in Physics Research Section A: Accelerators, Spectrometers, Detectors and Associated Equipment*, 499(2):624–632, 2003. The Relativistic Heavy Ion Collider Project: RHIC and its Detectors.

[20] H. Hahn *et al.*jevic, J. Wei, E. Willen, S. Ozaki, and S.Y. Lee. The rhic design overview. *Nuclear Instruments and Methods in Physics Research Section A: Accelerators, Spectrometers, Detectors and Associated Equipment*, 499(2):245–263, 2003. The Relativistic Heavy Ion Collider Project: RHIC and its Detectors.

[21] M. Harrison, T. Ludlam, and S. Ozaki. Rhic project overview. *Nuclear Instruments and Methods in Physics Research Section A: Accelerators, Spectrometers, Detectors and Associated Equipment*, 499(2):235–244, 2003. The Relativistic Heavy Ion Collider Project: RHIC and its Detectors.

[22] I Alekseev *et al.* Polarized proton collider at rhic. *Nuclear Instruments and Methods in Physics Research Section A: Accelerators, Spectrometers, Detectors and Associated Equipment*, 499(2):392–414, 2003. The Relativistic Heavy Ion Collider Project: RHIC and its Detectors.

[23] J. Adam and all. Longitudinal double-spin asymmetries for π^0s in the forward direction for 510 gev polarized pp collisions. *Phys. Rev. D*, 98:032013, Aug 2018.

[24] S. Bultmann et al. The PP2PP experiment at RHIC: Silicon detectors installed in Roman Pots for forward proton detection close to the beam. *Nucl. Instrum. Meth. A*, 535:415–420, 2004.

[25] J. Adam and all (The STAR collaboration). Measurement of the central exclusive production of charged particle pairs in proton-proton collisions at $$ \sqrt{s} $$= 200 gev with the star detector at rhic. *Journal of High Energy Physics*, 2020(7):178, 2020.

[26] M. I. Abdulhamid et al. Results on elastic cross sections in proton–proton collisions at s=510 GeV with the STAR detector at RHIC. *Phys. Lett. B*, 852:138601, 2024.

[27] J. KIRYLUK. Local polarimetry for proton beams with the star beam beam counters. In *Spin 2004*, page 718–721. WORLD SCIENTIFIC, August 2005.

[28] C. A. Whitten, Ahovi Kponou, Yousef I. Makdisi, and Anatoli Zelenski. The beam-beam counter: A local polarimeter at star. 2008.

[29] William B. Schmidke. Rhic polarization for runs 9-17. Technical report, Brookhaven National Lab. (BNL), Upton, NY (United States), 09 2018.

[30] Matteo Cacciari, Gavin P. Salam, and Gregory Soyez. Fastjet user manual: (for version 3.0.2). *The European Physical Journal C*, 72(3), March 2012.

[31] M. Anderson, J. Berkovitz, W. Betts, R. Bossingham, F. Bieser, R. Brown, M. Burks, M. Calderón de la Barca Sánchez, D. Cebra, M. Cherney, J. Chrin, W.R. Edwards, V. Ghazikhanian, D. Greiner, M. Gilkes, D. Hardtke, G. Harper, E. Hjort, H. Huang, G. Igo, S. Jacobson, D. Keane, S.R. Klein, G. Koehler, L. Kotchenda, B. Lasiuk, A. Lebedev, J. Lin, M. Lisa, H.S. Matis, J. Nystrand, S. Panitkin, D. Reichold, F. Retiere, I. Sakrejda, K. Schweda, D. Shuman, R. Snellings, N. Stone, B. Stringfellow, J.H. Thomas, T. Trainor, S. Trentalange, R. Wells, C. Whitten, H. Wieman, E. Yamamoto, and W. Zhang. The star time projection chamber: a unique tool for studying high multiplicity events at rhic. *Nuclear Instruments and Methods in Physics Research Section A: Accelerators, Spectrometers, Detectors and Associated Equipment*, 499(2–3):659–678, March 2003.

[32] W.J. Llope and all. The star vertex position detector. *Nuclear Instruments and Methods in Physics Research Section A: Accelerators, Spectrometers, Detectors and Associated Equipment*, 759:23–28, 2014.

[33] B. Abelev and all. Charged jet cross sections and properties in proton-proton collisions at $\sqrt{s}$ = 7TeV. *Phys. Rev. D*, 91:112012, Jun 2015.

[34] Torbjörn Sjöstrand, Stephen Mrenna, and Peter Skands. Pythia 6.4 physics and manual. *Journal of High Energy Physics*, 2006(05):026–026, May 2006.

[35] Peter Z. Skands. Tuning monte carlo generators: The perugia tunes. *Physical Review D*, 82(7), October 2010.

[36] Rene Brun, A. C. McPherson, Pietro Zanarini, M. Maire, and Flavienne Bruyant. Geant 3 : user's guide geant 3.10, geant 3.11. 1987.

[37] Torbjörn Sjöstrand, Stefan Ask, Jesper R. Christiansen, Richard Corke, Nishita Desai, Philip Ilten, Stephen Mrenna, Stefan Prestel, Christine O. Rasmussen, and Peter Z. Skands. An introduction to pythia 8.2. *Computer Physics Communications*, 191:159–177, June 2015.

[38] S. Agostinelli et al. GEANT4 - A Simulation Toolkit. *Nucl. Instrum. Meth. A*, 506:250–303, 2003.

[39] S. Gieseke, P. Kirchgaesser, and F. Loshaj. A new model for soft interactions in herwig. *Acta Physica Polonica B*, 48(6):1025, 2017.

[40] Roger Barlow. Systematic errors: facts and fictions, 2002.

[41] Gerald G. Ohlsen and P.W. Keaton. Techniques for measurement of spin-12 and spin-1 polarization analyzing tensors. *Nuclear Instruments and Methods*, 109(1):41–59, 1973.